World Journal of Experimental Biosciences

Volume 14, Number 1: 30 - 37
P-ISSN: 2313-3937, e-ISSN: 3070-0647
2026

Research article

Silver Nanoparticles from *Lawsonia inermis* against Uropathogenic *Escherichia coli*: Antimicrobial, Antibiofilm, and Molecular Docking Investigations

Jenan Atiyah Ghafil[1]*, Dongmei Li[2], Deyar Jassim Shawi[1], Nabaa Amer Jaber[1]

ABSTRACT

Uropathogenic *Escherichia coli* (UPEC) is responsible for more than 80% of urinary tract infections (UTIs). These infections are associated with multidrug resistance, especially to extended-spectrum beta-lactamases (ESBL). This study evaluated the antibacterial and antibiofilm potential of biogenic silver nanoparticles (Bio-AgNPs) synthesized using *Lawsonia inermis* (henna) leaf extract against multidrug-resistant UPEC isolates. The virulence (fimH and papC) and resistance genes (blaCTX-M and blaKPC) in UPEC were amplified using multiplex PCR. The study also explores their mechanism of action and their molecular docking with three key UPEC virulence targets. The *fimH* gene was found in all isolates, while *papC* was found only in four isolates. The study showed that *blaCTX-M* and *blaKPC* genes were present in 4 and 1 isolate from 7 studies, respectively. Synthesized bio-AgNPs were semi-spherical (less than 50 nm). Bio-AgNPs exhibited potent, concentration-dependent bactericidal activity against all seven UPEC isolates (MICs of 3.12–12.5 µg/mL; MBCs of 6.25–25.0 µg/mL). All UPEC isolates were strong or moderate biofilm producers; minimum biofilm inhibitory concentration (MBIC) and minimum biofilm eradication concentration (MBEC) values were 4–64 times higher than planktonic MIC values. Molecular docking demonstrated strong binding affinities of the bio-AgNP silver core (−9.84 to −11.32 kcal/mol) and lawsone (−6.94 to −8.45 kcal/mol) against FimH adhesin (PDB: 4XO8), PapC usher (PDB: 3RFZ), and DNA Gyrase B (PDB: 4DUH), outperforming reference ligands. These findings support the use of bio-AgNPs synthesized as a promising alternative therapeutic strategy against multidrug-resistant (MDR) UPEC-associated UTIs. This finding needs an *in vivo* improvement project.

Keywords: Antibiofilm, DNA gyrase, FimH, Green nanotechnology, *Lawsonia inermis*, Molecular docking, Silver nanoparticles, Uropathogenic *Escherichia coli*.

Citation: Ghafil JA, Li D, Shawi DJ, Jaber NA. (2026) Silver Nanoparticles Synthesized from *L. inermis* against Uropathogenic *Escherichia coli*: Antimicrobial, Antibiofilm, and Molecular Docking Investigations. *World J Exp Biosci* 14:30-37. doi: 10.65329/wjeb.v14.01.06

Received May 10, 2026; Revised June 17, 2026; Accepted: June 19, 2026; Published: June 25, 2026

1. INTRODUCTION

It is well known that Urinary tract infections (UTIs) are the most common infections worldwide. Uropathogenic *Escherichia coli* (UPEC) is responsible for a large proportion of UTIs [1]. UPEC is particularly problematic because it can express different virulence factors that help adhesion of bacteria to the epithelial cells of urinary tract tissues, invasion of host epithelial cells, and

* Correspondence: **Dr. Jenan A. Ghafil.** E-mail: genan.atiyah@sc.uobaghdad.edu.iq
Department of Biology, College of Science, University of Baghdad, Baghdad, 10071, Iraq
: **Dr. Dongmei Li**. E-mail: dl33@georgetown.edu
Department of Microbiology & Immunology, Georgetown University Medical Center, Washington, D.C.20057, USA.

Full list of author information is available at the end of the article.

colonization on the surface for a long time [2]. The significant factor contributing to the persistence of bacterial infection is biofilm production. The bacterial cells are embedded within a self-produced extracellular polymeric matrix. This biofilm lifestyle enhances bacterial tolerance to antibiotics and immune defenses, making infections difficult to cure and leading to chronic disease [3].

There is a continued increase in the number of multidrug-resistant (MDR) *E. coli* strains, leading to an increase in the global burden associated with UTIs [4]. Conventional antibiotics are becoming ineffective, therefore there is an immediate requirement for new and exciting antimicrobial methods. Nanotechnology has recently emerged as a viable new area for developing novel antimicrobial agents. Of these types of nanomaterials, silver nanoparticles (AgNPs) are gaining attention for their very strong, broad-spectrum antibacterial properties because they cause damage to cell membranes, generate oxidative stress in microorganisms and disrupt all major types of biomolecules that are necessary for the survival of microbes [5].

The green synthesis of nanoparticles from plant extracts represents a more sustainable and environmentally friendly method of producing nanoparticles compared to traditional chemical and physical synthesis methods. This method utilises the naturally occurring phytochemicals found in plants for the reduction and stabilisation of nanoparticles, thereby eliminating the need for toxic reagents and often increasing the biological activity of resulting nanoparticles [6]. *Lawsonia inermis* (henna) is a well-established medicinal plant that has demonstrated antimicrobial, antioxidant, and anti-inflammatory activities. The diverse range of phytochemicals found in henna, such as lawsone, flavonoids, tannins, and phenolic compounds, enables the biosynthesis of AgNPs that are effective antimicrobial agents [7].

The previous published literature reported that zinc oxide nanoparticle (ZnO NPs) was bio-synthesized using *L. inermis* leaf extract and the antibacterial and antibiofilm activities of these nanoparticles were evaluated against different isolates of UPEC [8]. The earlier study evaluated the antibiofilm and antibacterial activities of biosynthesized AgNPs by checking the efficacy of this nanoparticle in disrupting the bacterial biofilm [9]. Virtual molecular docking studies were conducted in prior work to evaluate potential interactions between major plant-derived compounds and key bacterial proteins central to bacterial virulence and biofilm formation. By combining experimental and computational approaches, this work provides deeper insight into the antimicrobial mechanisms of biosynthesis AgNPs. The objective of the current study is to highlight the above gaps related to the bactericidal, antibiofilm, and mechanistic aspects of biosynthesis-derived AgNPs.

2. MATERIALS AND METHODS

2.1. Bio-AgNP Synthesis

The leaves of the plant (*L. inermis*) were obtained from the Department of Biology, College of Science, University of Baghdad, Baghdad, Iraq. A 10% (w/v) aqueous extract was prepared by heating dried leaf powder in distilled water at 80°C for 30 min. The mixture was filtered to obtain a clear extract. Ten millimeters of the clear plant extract was added to 90 mL of 1 mM silver nitrate ($AgNO_3$; Sigma-Aldrich, USA). The mixture was mixed by using magnetic stirred at 60°C for 4 h in the dark field. The indication of nanoparticles formation by a visible color change. The mixture was centrifuged at 12,000 rpm for 15 min, and the pellet was washed three times with sterile double-distilled water. The purified AgNPs were stored at 4°C.

Bio-AgNP formation was confirmed by UV-Vis spectroscopy (300–700 nm). Morphology and size were determined by scanning electron microscope (SEM) (MIRA3 TE Scan, China). The prepared Ag NPs were characterized using atomic force microscopy (AFM; Innova® AFM; Bruker, Santa Barbara, USA). For AFM analysis, a thin film of the nanoparticles was deposited on a silica glass plate.

2.2. Bacterial Strains and Identification

Clinical isolates of UPEC were collected from patients at Baghdad Teaching Hospital (2024–2025). The bacterial isolates were cultured on selective and differential media, including MacConkey agar and eosin methylene blue agar. Additionally, specific biochemical tests were performed. Bacterial cell morphology after Gram staining was assessed to identify bacterial species. The identification of bacterial species was confirmed using the VITEK® 2 Gram-Negative identification card (GN) (BIOMÉRIEUX, France).

2.3. Antibiotic susceptibility

The standard Kirby–Bauer disk diffusion method was used to determine the susceptibility of UPEC to the following antibiotics: Ampicillin (AMP, 10 µg), Ciprofloxacin (CIP, 5 µg), Nitrofurantoin (NIT, 300 µg), Gentamicin (GEN, 10 µg), Amikacin (AMK, 30 µg), and Imipenem (IPM, 10 µg). Antibiotic susceptibility testing was also performed after culture on Mueller–Hinton Agar (MHA, Hi-Media, India). The instructions of the Clinical and Laboratory Standards Institute (CLSI, 2023) were followed to interpret the results [10].

2.4. PCR method

A multiplex PCR with specific gene primers was used to detect virulence genes (fimH and papC) and resistance genes (blaCTX-M, blaKPC) in UPEC. The conditions of experiment were standardized before starting the experiment. Amplified products were verified by agarose gel electrophoresis and purified for subsequent Sanger sequencing to ensure the specificity and accuracy of each gene product [11].

2.5. Minimum Inhibitory and Bactericidal Concentrations

The minimum inhibitory concentrations (MICs) were determined by the broth microdilution method in cation-adjusted Mueller–Hinton broth (CAMHB) according to CLSI 2023 guidelines. Hundred microliters of serial two-fold dilutions of Bio-AgNPs ranging from 400 to 0.39 µg/mL were made by MHB (Hi media, India) in Nunc™ 96-Well Polystyrene Conical Bottom MicroWell™ Plates, then mixed with 5 µL of 10^8 CFU/mL of testing UPEC isolate. Growth inhibition was visualized after 18 hours culture at 37°C. Minimum Bactericidal Concentration (MBC) was determined by no-visible growth in subcultures on MHB agar from growth-negative wells. Selectivity index (SI) was calculated as CC_{50} (HEK-293) / MIC.

2.6. Biofilm Formation and Antibiofilm Activity

The standard method of Al-Mutalib & Zgair (2023) was followed to measure the biofilm formation of UPEC isolates. Biofilm formation was quantified by crystal violet (CV) staining (OD_{590}).

Isolates were classified as non-biofilm (OD ≤ 2× control), weak, moderate, or strong producers [10]. Minimum Biofilm Inhibitory Concentration (MBIC) and Minimum Biofilm Eradication Concentration (MBEC) were determined against preformed 24-hour biofilms exposed to serial dilutions of Bio-AgNP. Biofilm inhibition and disruption at MIC, 2×MIC, and 4×MIC were quantified using CV biomass and expressed as % reduction relative to untreated controls (two-way ANOVA).

2.7. Time-Kill Kinetics

Time-kill assays were performed with UPEC isolates at MIC, 2×MIC, and 4×MIC. Aliquots (100 µL) were collected at 0, 15, 30 min, and 1, 2, 4, 6, 8, 12, and 24 hours, plated in triplicate on brain heart infusion (BHI, Hi-media, India) agar, and incubated for 24 hours at 37°C. Bactericidal activity: ≥3 $\log_{10}$ (≥99.9%) reduction in initial CFU/mL.

2.8. Molecular Docking

2.8.1. Protein and Ligand Preparation

Three UPEC targets were selected: FimH adhesin (PDB: 4XO8), PapC usher (PDB: 3RFZ), and DNA Gyrase B (PDB: 4DUH). Structures were prepared in AutoDockTools 1.5.7 (removal of water molecules, addition of Gasteiger charges, PDBQT format). Grid box dimensions: 25 × 25 × 25 Å (spacing 0.375 Å). Ligands tested: Bio-AgNP Ag^+ core and lawsone (PubChem CID: 10685). References: ciprofloxacin and novobiocin. Docking performed using AutoDock Vina 1.2.0 (exhaustiveness = 20). Visualization: UCSF ChimeraX 1.6 and Discovery Studio Visualizer 2021.

2.9. Statistical analysis

Statistics were analyzed using OriginPro by OriginLab Corporation in the United States. Each experiment was repeated three times, and therefore, valid means were used for the analysis. Results were expressed as a mean value plus or minus one standard deviation (SD). To compare the means of different experimental groups, statistical analysis was performed using one-way and/or two-way ANOVAs; if significant results were found, appropriate post hoc tests were used to determine which experimental group means differed significantly from one another. A threshold of $p < 0.05$ was used to indicate statistical significance. Dose–response and time–dose response curves were created using Origin software.

3. RESULTS

3.1. Characterization of Bio-AgNPs

The present study demonstrated that L. inermis extracts reduced $AgNO_3$ within 30–45 minutes, as indicated by a color change from pale yellow to reddish-brown. UV-Vis spectroscopy revealed a surface plasmon resonance (SPR) peak at 418 nm, confirming the formation of silver nanoparticles (AgNPs).

SEM analysis showed well-dispersed, semispherical nanoparticles, and most particle diameters were <50 nm. The SEM showed that the range of prepared particles was 65–15, and the mean was 38 ± 11.5. The AFM showed that most prepared bio-AgNPs were less than 50 nm. The study clearly showed that the procedure used for preparing biosynthesized silver nanoparticles was a highly efficient method because the yielded particles were typically nanoparticles.

3.2. Characteristics and Resistance Profiles of Seven Clinical Isolates

All seven isolates exhibited multidrug resistance. Resistance to ampicillin was observed in all isolates (7/7). However, resistance to fosfomycin was observed in one isolate only (1/7). The study also showed that six isolates were resistant to ciprofloxacin and four to nitrofurantoin. The *blaCTX-M* gene was detected in 4 of the 7 isolates, while *blaKPC* was found in one isolate (UE-07). The *fimH* gene was present in all isolates, whereas *papC* was detected in 5 of the 7 isolates. Notably, all *papC*-positive isolates demonstrated strong biofilm production (Table 1).

Table 1. Clinical isolate characteristics, antibiotic resistance profiles, and virulence gene carriage. AMP: ampicillin; CIP: ciprofloxacin; TMP-SMX: trimethoprim-sulfamethoxazole; GEN: gentamicin; NIT: nitrofurantoin; FOF: fosfomycin; AMK: amikacin.

Isolate	Source	Resistance Profile	blaKPC	blaCTX-M	fimH / papC
UE-01	Midstream urine	AMP, CIP, TMP-SMX, NIT	−	−	+ / +
UE-02	Catheter urine	AMP, CIP, GEN, TMP-SMX	−	+	+ / +
UE-03	Midstream urine	AMP, CIP, NIT, FOF	−	+	+ / −
UE-04	Catheter urine	AMP, CIP, TMP-SMX, AMK	−	−	+ / +
UE-05	Blood culture	AMP, CIP, GEN, TMP-SMX, NIT	−	+	+ / +
UE-06	Midstream urine	AMP, GEN, TMP-SMX, FOF	−	−	+ / −
UE-07	Catheter urine	AMP, CIP, NIT, GEN, AMK	+	+	+ / +

3.3. Bio-AgNPs Antibacterial Activity

Minimum inhibitory concentration (MIC), minimum bactericidal concentration (MBC), and selectivity index of Bio-AgNPs were evaluated against all UPEC isolates. Bio-AgNPs exhibited significant antibacterial activity against all UPEC strains (Table 2). The MIC values ranged from 3.12 µg/mL to 12.5 µg/mL for UE-07, the *blaKPC*-positive isolate, when referred to 12.5 µg/mL in UE-7 strain. Similarly, the MEC values ranged from 6.25 µg/mL to 25µg/mL. The MBC/MIC ratios were ≤ 4 for all isolates, confirming the bactericidal mechanism of Bio-AgNPs. Cytotoxicity analysis revealed a CC_{50} value of 49.9 µg/mL, while the selectivity index (SI) values ranged from 8.0 to 16.0. When ESBL-positive isolates did not exhibit significantly higher resistance to Bio-AgNP, consistent the hypothesis that Bio-AgNPs exert antibacterial effects through a multi-target, non-antibiotic mechanism.

Table 2. Minimum inhibitory concentration (MIC), minimum bactericidal concentration (MBC), MBC/MIC ratio, and selectivity index of Bio-AgNPs against all UPEC isolates.

Isolate	MIC (µg/mL)	MBC (µg/mL)	MBC/MIC Ratio	Bactericidal	Selectivity Index*
UE-01	3.12	6.25	2	Yes	16.0
UE-02	3.12	12.5	4	Yes	16.0
UE-03	6.25	12.5	2	Yes	8.0
UE-04	3.12	6.25	2	Yes	16.0
UE-05	6.25	25.0	4	Yes	8.0
UE-06	3.12	6.25	2	Yes	16.0
UE-07	12.5	25.0	2	Yes	8.0

Selectivity Index (SI) = CC_{50} (HEK-293 cells) / MIC. Values represent means of three independent experiments in triplicate. High SI (e.g., 16–32): strong antibacterial effect with low toxicity (desirable). Moderate SI (8–16): acceptable but needs caution. Low SI (≤4): narrow safety margin (potential toxicity concern).*

3.4. Biofilm Formation and Antibiofilm Activity

The biofilm formation capacity varied among the UPEC clinical isolates, with five of the seven isolates classified as strong biofilm producers (OD_{570} > 0.68), while the remaining two were identified as moderate producers (Table 3). The minimum biofilm inhibitory concentration (MBIC) values ranged from 12.5 µg/mL to 50.0 µg/mL (4–8× MIC), whereas the minimum biofilm eradication concentration (MBEC) was ≥ 200 µg/mL for 5 of the 7 clinical isolates, highlighting the high tolerance of established UPEC biofilms.

Table 3. Biofilm formation capacity, classification, minimum biofilm inhibitory concentration (MBIC), minimum biofilm eradication concentration (MBEC), and MBEC/MIC ratio for Bio-AgNP treatment of UPEC isolates.

Isolate	OD570 (Mean ± SD)	Biofilm Class	MBIC (µg/mL)	MBEC (µg/mL)	MBEC/ MIC Ratio
UE-01	0.89 ± 0.07	Strong	25.0	200	64.102
UE-02	0.77 ± 0.06	Strong	25.0	200	64.102
UE-03	0.62 ± 0.05	Moderate	12.5	100	16
UE-04	0.91 ± 0.08	Strong	25.0	400	128.20
UE-05	1.04 ± 0.09	Strong	50.0	400	64
UE-06	0.55 ± 0.04	Moderate	12.5	100	32.051
UE-07	0.98 ± 0.10	Strong	50.0	400	32

A clear concentration-dependent inhibitory effect on biofilm formation was observed, as shown in Fig. 1. The effect of varying concentrations of AgNPs on biofilm production was evaluated by as measuring OD 590 nm. As the concentration of Bio-AgNPs increased from 1/32 MIC to 1/2 MIC, the optical density values progressively decreased, indicating reduced biofilm formation. By contrast, the untreated control groups consistently exhibited the highest OD_{590} values, confirming robust biofilm production under normal growth conditions.

However, while sub-inhibitory concentrations of Bio-AgNPs (1/32 and 1/16 MIC) reduced biofilm formation compared with the control groups, higher sub-MIC concentrations (1/8, 1/4, and 1/2 MIC) produced markedly greater inhibition. These findings indicate that Bio-AgNPs can significantly impair bacterial adhesion and extracellular matrix production, thereby inhibiting biofilm development even at concentrations below the MIC.

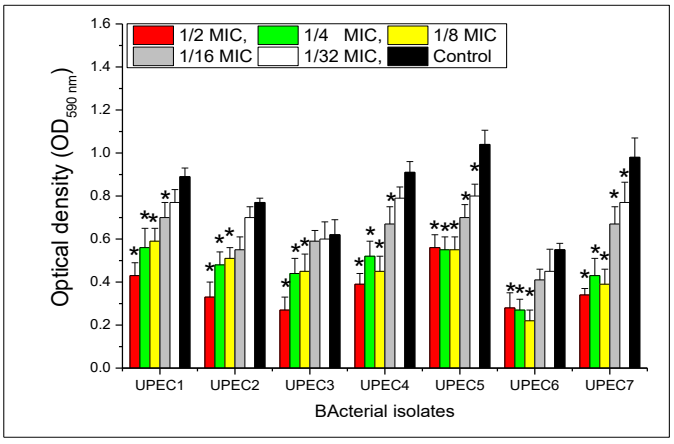

Fig. 1. Impact of sub-inhibitory concentrations (sub-MICs) of AgNPs (½ MIC, ¼ MIC, $^1/_8$ MIC, $^1/_{16}$ MIC, and $^1/_{32}$ MIC) on biofilm formation of seven isolates of uropathogenic E. coli (UPEC) (UPEC1- UPEC7). Biofilm biomass was quantified using the crystal violet microtiter plate assay and measured at 590 nm (OD_{590}). Results demonstrate a concentration-dependent reduction in biofilm formation compared with the control (isolates treated with PBS). Asterisks indicate a significant difference from the controls.

3.5. Time-Kill Kinetics

The bactericidal time course of AgNPs against six isolates of uropathogenic *E. coli* (UPEC1, UPEC2, UPEC3, UPEC4, UPEC5, and UPEC7) showed a concentration- and time-dependent effect (killing time). While the growth of untreated isolates (control groups) remained stable or increased slightly over the 30-h incubation period, 6.5-8.1 $\log_{10}$ CFU/mL, bacterial counts declined gradually across all tested isolates treated with AgNPs at MIC, 2 x MIC, and 4 x MIC concentrations). The decline accelerated over time, with very low levels of bacterial growth by the end of the experiment (approximately 0–1 $\log_{10}$ CFU/mL at 25–30 h). Notably, effective killing showed a slower rate than at higher concentrations. Exposure to double MIC resulted in a more rapid decrease in viable bacterial counts. The most isolates showed a sharp decline within the first 5–15 h and near-complete eradication of viable cells by approximately 20–25 h. This pattern was also observed under 4 × MIC of AgNPs condition. These findings demonstrated that AgNPs exhibit bactericidal activity against UPEC isolates. Increasing the concentration from MIC to 2×MIC and 4×MIC significantly accelerates bacterial killing.

3.6. Molecular Docking Results

To evaluate the interactions among active components responsible for antibacterial activity, molecular docking simulations were done. Three-dimensional binding poses of the bio-AgNP (Ag^+ core) and its associated capping agent, lawsone, were mapped against three serious bacterial targets. The key spatial direction of the Ag^+ core is shown in **Table 4** and Fig. 3.

3.6.1. Binding to FimH Adhesin (PDB: 4XO8).

The adhesion of bacteria (FimH) is a crucial virulence factor that mediates beginning bacterial adhesion to host cell surfaces. As shown in the structural outline and magnified inset of **Fig.3A**, the bio-AgNP core showed a highly favorable, strong binding affinity within the FimH mannose-binding lectin domain (ΔG = −9.84 kcal/mol, Ki = 68.3 nM). The visualization clearly demonstrates a multi-dentate coordination sphere around the central Ag^+ ion, driven by robust electrostatic and hydrogen-bonding interactions with key polar residues, specifically Asp140, Asn163, and Asp162. The binding is stabilized by central hydrophobic contacts with Phe1 and Ile13, anchoring the nanoparticle core firmly within the pocket. Lawsone also exhibited significant binding in this region (ΔG = −7.21 kcal/mol, Ki = 5.40 µM), interacting predominantly with Tyr48, Gln133, and Asp140. Both the Ag^+ core and the bio-capping agent substantially outperformed the reference antibiotic, CIP (ΔG = −5.63 kcal/mol, Ki = 73.2 µM), at this non-classical antibacterial target, indicating a strong antiadhesive mechanism.

3.6.2. Binding to PapC Usher (PDB: 3RFZ)

PapC usher protein is an integral membrane channel essential for the assembly and translocation of P-fimbriae. The Bio-AgNP Ag^+ core exhibited profound binding affinity for this target (ΔG = −10.17 kcal/mol, Ki = 36.8 nM). **Fig. 3B** shows that the spherical silver core closely corresponds to PapC plug domain. The region responsible for gating pilus subunit translocation. The predictive model shows direct, stabilizing interactions with an array of amino acids, including Arg651, Phe628, Thr632, Asp636, and Glu620. Furthermore, Lawsone showed moderate affinity for this site (ΔG = −6.94 kcal/mol, Ki = 8.70 µM). In stark contrast, ciprofloxacin scored only −5.01 kcal/mol, confirming a distinct, non-quinolone binding mode for the synthesized nanoparticles that likely sterically blocks the PapC channel and impedes fimbriogenesis.

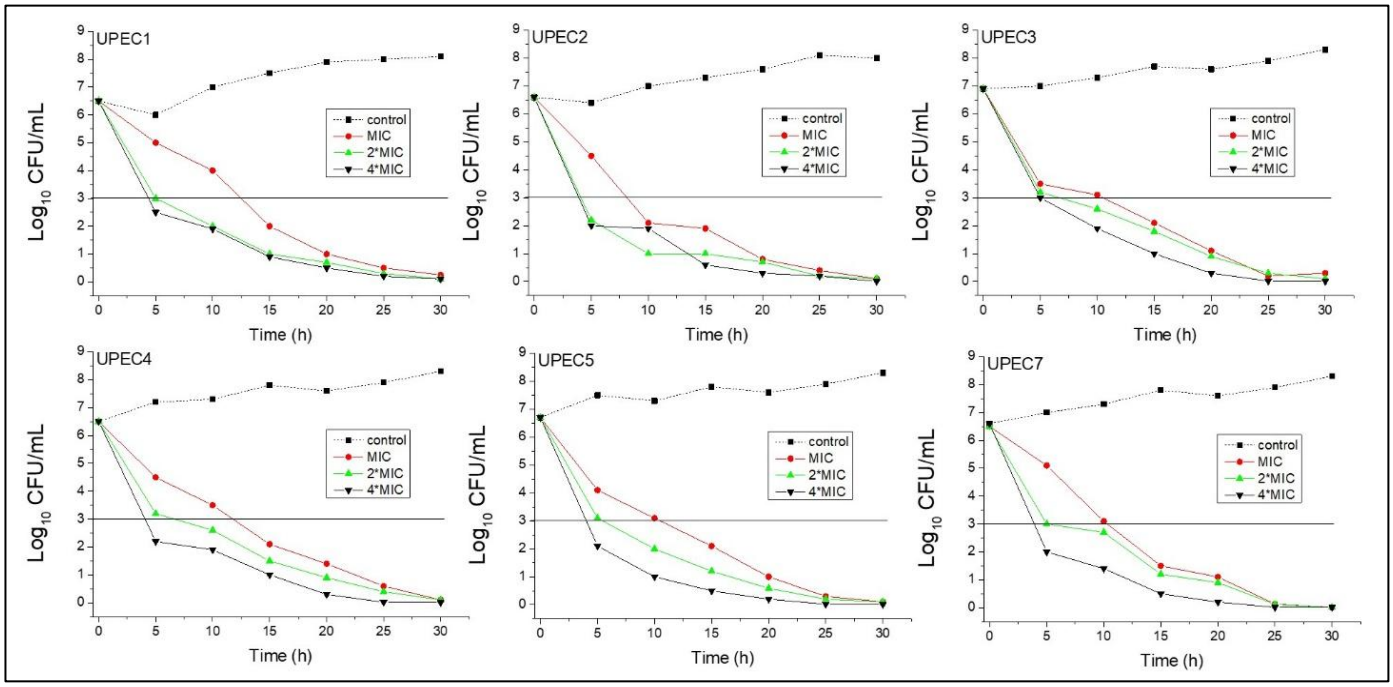

Fig. 2. Time course of bactericidal activity of AgNPs against six isolates of UPEC (UPEC1, UPEC2, UPEC3, UPEC4, UPEC5, and UPEC7) was evaluated over 30 h after exposure to two concentrations of AgNPs (MIC, 2×MIC, and 4×MIC). The number of viable bacteria, expressed as CFU/mL, was reported and compared with untreated controls.

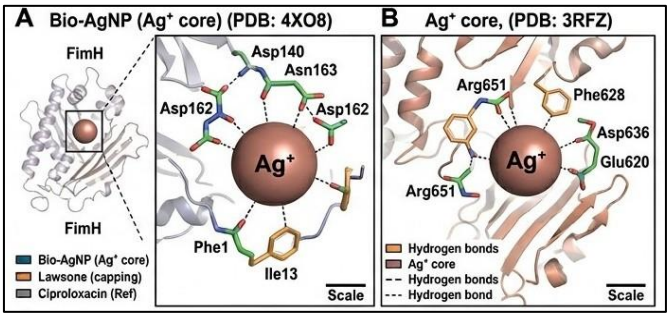

Fig. 3. Virtual molecular docking evaluation of silver ion linking within a bio-AgNP and an exchange protein site. (A) Bio-docking of Ag+ ion (core) with FIMH (PDB: 4X08), showing the full protein structure (left) and a magnified view of the interaction pocket (right). The core residues (labeled Asp140, Asn163, Asp162, Phe1, and Ile13) are around the central silver ion (Ag^+). The legend for this panel details bio-AgNP, Lawsone (capping), and the reference for ciprofloxacin. (B) Alternative comparative site for an Ag+ ion (core) within another protein structure (PDB: 3RFZ). Interactions involve residues Arg651, Phe628, Asp636, and Glu620. The legend for this panel identifies hydrogen bonds, the Ag^+ core, and dashed interaction lines.

3.6.3. Binding to DNA Gyrase B (PDB: 4DUH)

The highly interesting virtual result was seen against DNA Gyrase B, an enzyme crucial forbacterial DNA replication and supercoiling. The bio-AgNP (Ag+ ion (core)) showed remarkably high binding at the catalytic ATP-binding site (ΔG = −11.32 kcal/mol, Ki = 6.45 nM). In this study, a direct comparison of this binding pocket was visualized (Fig 4). Fig 4A shows the highly efficient spatial accommodation of the Ag^+ core that forms a compact network of interactions of Asp73, Asn46, Lys103, Ile78, and Gly77. These are the matching critical residues that were engaged by the known Gyrase B inhibitor novobiocin, shown side-by-side in Fig 4B (Ki = 189 nM). The Ag^+ ion (core) interaction shows a predicted binding affinity approximately 29-fold higher than that of novobiocin (Quantitatively). Additionally, lawsone showed potent binding at this site (ΔG = −8.45 kcal/mol, Ki = 0.63 μM) independently. The structural and thermodynamic data suggest that the biosynthesized AgNPs act as highly potent, two-action competitive inhibitors of DNA Gyrase B.

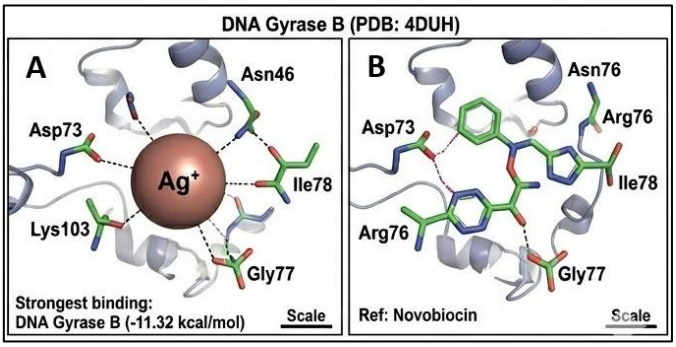

Fig 4. The image shows molecular docking of biosynthesized AgNP components at UPEC target binding sites. Three-dimensional molecular docking images of the bio-AgNP (Ag^+ ion core) within the active binding pockets of precious bacterial target proteins. The present figure shows the comparative docking analysis within the ATP-binding site of DNA Gyrase B (PDB: 4DUH). Panel A shows the strong binding of the Ag^+ ion (core), representing the strongest affinity observed in the study (ΔG = -11.32 kcal/mol), which is anchored by Asp73, Asn46, Lys103, Ile78, and Gly77. This is compared directly alongside the reference inhibitor novobiocin (B). Dashed lines denote predicted intermolecular interactions and coordination within the respective binding cavities.

4. DISCUSSION

In recent years, several studies have highlighted that resistance among pathogenic and opportunistic bacteria to a wide spectrum of antibiotics is a serious public health problem and represents a major challenge [13,14].

Table 4. Molecular docking binding energies (ΔG, kcal/mol), inhibition constants (Ki), and key interacting residues for Bio-AgNP (Ag^+ core) and lawsone against FimH, PapC, and DNA Gyrase B. Ciprofloxacin and novobiocin are reference ligands.

Target Protein	Ligand	Binding Energy (kcal/mol)	Inhibition Constant (Ki)	Key Interacting Residues
FimH (PDB: 4XO8)	Bio-AgNP (Ag^+ core)	−9.84	68.3 nM	Asp140, Asn163, Asp162, Phe1, Ile13
FimH (PDB: 4XO8)	Lawsone (capping)	−7.21	5.40 μM	Tyr48, Gln133, Asp140, Ile13
FimH (PDB: 4XO8)	Ciprofloxacin (Ref)	−5.63	73.2 μM	Asp140, Phe1, Asn163
PapC (PDB: 3RFZ)	Bio-AgNP (Ag^+ core)	−10.17	36.8 nM	Arg651, Phe628, Thr632, Asp636, Glu620
PapC (PDB: 3RFZ)	Lawsone (capping)	−6.94	8.70 μM	Arg651, Asp636, Lys631
PapC (PDB: 3RFZ)	Ciprofloxacin (Ref)	−5.01	212 μM	Arg651, Thr632
DNA Gyrase B (PDB: 4DUH)	Bio-AgNP (Ag^+ core)	−11.32	6.45 nM	Asp73, Asn46, Lys103, Ile78, Gly77
DNA Gyrase B (PDB: 4DUH)	Lawsone (capping)	−8.45	0.63 μM	Asp73, Asn46, Arg76, Thr165
DNA Gyrase B (PDB: 4DUH)	Novobiocin (Ref)	−9.22	189 nM	Asp73, Asn46, Arg76, Ile78, Gly77

Thus, a recent study suggested alternative methods, either by improving antibiotics through combinations with different materials to enhance their antibacterial activity [15], or by using other antimicrobial agents such as herbal extracts [12] and polymeric or metallic nanoparticles [16]. Various studies have reported the antibacterial efficacy of AgNPs against multiple pathogenic bacterial species [17]. The mechanism by which AgNPs affect bacterial attachment and biofilm formation needs to be explained; thus, the present study aims to highlight the antibacterial effectiveness of bio-AGNPs against uropathogenic *E. coli*. Furthermore, the present study visualized the molecular docking of interactions between silver ions and two proteins important in bacterial attachment and biofilm formation, as well as another protein important in bacterial survival (DNA Gyrase B).

The physicochemical profile of the synthesized Bio-AgNPs, the SPR peak at 418 nm, and a mean diameter of less than 50 nm post examining the prepared AgNPs under SEM. Al these tests confirming the monodisperse nanoparticles consistent with lawsone- and flavonoid-mediated bioreduction and surface capping. The nanoscale size of AgNPs confers a high surface-area-to-volume ratio, maximizing Ag^+ release flux across bacterial membranes [18]. All seven UPEC clinical isolates were MDR, with co-detection of *fimH* and *papC* virulence genes in strong biofilm producers, corroborating the well-established role of P-fimbriae in mediating surface attachment and biofilm initiation [19].

Biosynthesized AgNPs exhibited high bactericidal activity against all study isolates (MIC 3.12–12.5 μg/mL; MBC/MIC ≤ 4), and this was independent of ESBL, indicating that the mechanism of action targets, membrane-disruptive bypasses of conventional β-lactamase-mediated resistance [20]. Selectivity indices of 8.0–16.0 indicate an acceptable therapeutic window for the intended topical urinary application [21]. The result of the present study is in line with a previous study that reported bio-AgNPs activity against uropathogenic *E. coli* [22]. The current study showed that UPEC biofilm tolerance was MBEC ≥200 μg/mL in 5/7 isolates, due to EPS matrix diffusion barriers and persistent cell populations [23]. However, sub-MICs produced concentration-dependent biofilm inhibition (Figure 1) by suppressing *fim* gene expression and fimbrial biogenesis, blocking surface colonization before mature biofilm architecture is built [24, 25]. Time-course kill assays confirmed ≥3 $\log_{10}$ bactericidal reductions. The faster kinetics were observed at higher concentrations (4×MIC: eradication within 15–20 h), consistent with a multi-hit model that requires cytoplasmic Ag^+ accumulation to reach a threshold for irreversible multi-target damage [26].

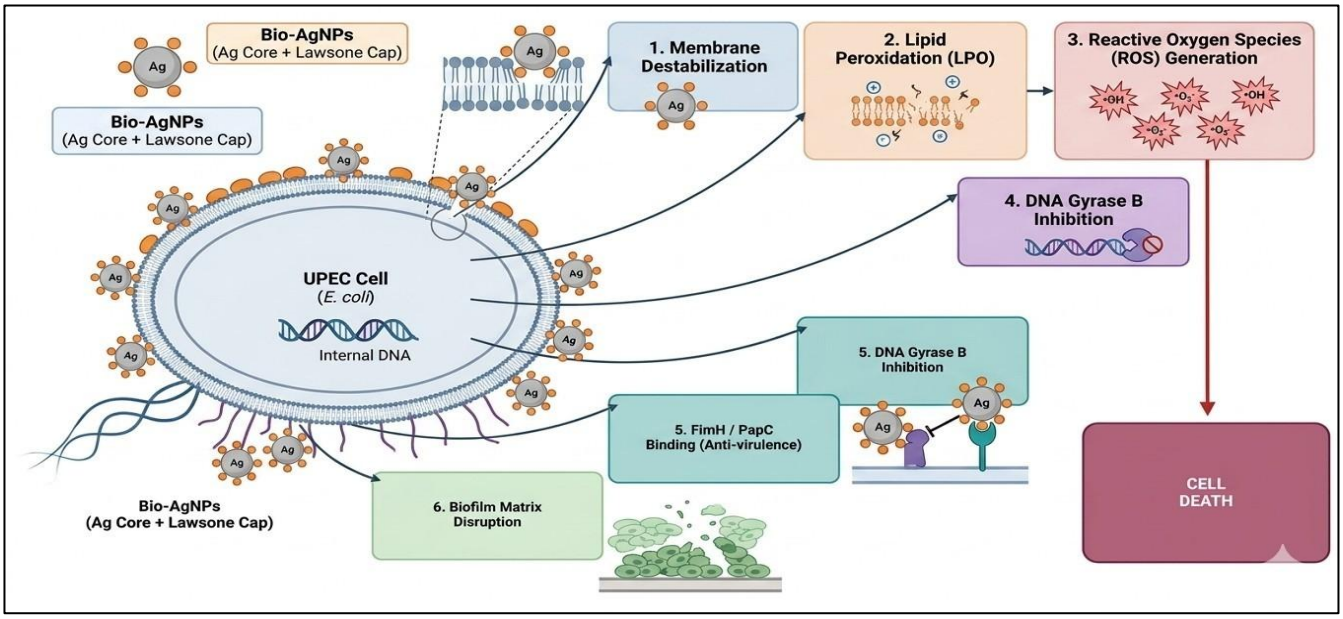

Fig.5. Proposed multi-target mechanism of Bio-AgNPs against UPEC, illustrating membrane destabilization, ROS-mediated lipid peroxidation, anti-virulence target binding, and DNA Gyrase B inhibition, culminating in bacterial cell death. This Figure Proposed Mechanism of Action of Bio-AgNPs Against Uropathogenic E. coli (UPEC) Schematic summarizing the multi-target antibacterial mechanism: ① membrane destabilization, ② lipid peroxidation, ③ ROS generation, ④ DNA Gyrase B inhibition (anti-replication), ⑤ FimH/PapC binding (anti-virulence/anti-adhesion), and ⑥ biofilm matrix disruption, collectively leading to UPEC cell death.

Figure 5 integrates these findings into a six-node mechanistic model. Ag^+ ions released from the nanoparticle surface (①) destabilize the bacterial membrane by binding thiol groups and dissipating the proton motive force, triggering (②) Fenton-like lipid peroxidation and (③) intracellular ROS amplification that collectively inactivate DNA, enzymes, and structural proteins [26, 27, 28]. Computationally, (④) DNA Gyrase B inhibition is supported by the highest docking affinity recorded (ΔG = −11.32 kcal/mol, Ki = 6.45 nM at the catalytic Asp73 residue), representing 29-fold greater predicted affinity than novobiocin [29]. Anti-virulence targeting of (⑤) FimH (ΔG = −9.84 kcal/mol) and (⑥) PapC (ΔG = −10.17 kcal/mol) provides a resistance-sparing mode of action by disarming adhesion and pilus assembly without bactericidal lethal pressure [30]. Biofilm matrix disruption completes the model and is consistent with the significant antibiofilm activity observed across all tested concentrations [24].

The present study demonstrated that *L. inermis*-derived Bio-AgNPs exhibit potent, multi-mechanistic antibacterial and antibiofilm activity against MDR UPEC, collectively explained by the model depicted in Fig 5 and supported by molecular docking analyses of three clinically relevant virulence targets. While *in vivo* validation in murine UTI models is required to bridge the translational gap, these data position Bio-AgNPs as a promising candidate strategy for managing biofilm-associated MDR urinary tract infections in the post-antibiotic era [31].

5. CONCLUSION

The present study demonstrated the antibacterial and antibiofilm effect of biosynthesized AgNPs from *L. inermis* against MDR UPEC, including ESBL and KPC-producing isolates. The MICs of bio-AgNPs ranged from 3.12 to 12.5 µg/mL. The bactericidal MBC/MIC ratios were less or equal to 4 across all studied isolates. The selectivity indices ranged from 8 to 16, indicating a safety margin for the AgNPs. The study showed that the sub-MICs reduced biofilm formation in a concentration-dependent manner. The AgNPs time-killing was also concentration-dependent. Molecular docking revealed that the Ag^+ core and lawsone strongly inhibited three critical UPEC targets (FimH, PapC, and DNA Gyrase B), outperforming ciprofloxacin and novobiocin at their respective binding sites. The findings of the current study suggest that bio-AgNPs are a promising multi-target therapeutic candidate against drug-resistant UTI.

Acknowledgments

At this stage, I would like to thank the staff of all hospitals in Baghdad Governorate for their assistance in collecting the clinical samples.

Funding information

This work received no specific grant from any funding agency.

Conflict of interest

The authors declare no conflicts of interest.

Ethical Approval

This review was approved by the Scientific Committee of the University of Baghdad, Baghdad, Iraq, and the Ministry of Health (1104; 16-04-2025).

Author contributions

Ghafil JA: Conceptualization; Data curation; Formal analysis; Investigation; Methodology; Project administration; Resources; Supervision; Roles/Writing - original draft; and Writing - review & editing.

Li D.: Formal analysis; Roles/Writing - original draft; Visualization; Writing - review & editing.

Shawi DJ: Investigation; Methodology; Resources; Visualization.

Jaber NA: Investigation; Project administration; Supervision; Validation.

Data availability

Data will be made available on request.

6. REFERENCES

[1] **Mancuso G, Midiri A, Gerace E, Marra M, Zummo S, Biondo C.** (2023) Urinary Tract Infections: The Current Scenario and Future Prospects. *Pathogens (Basel, Switzerland)*, **12**(4), 623. doi: 10.3390/pathogens12040623, PMCID: PMC10145414

[2] **Azimzadeh PN, Birchenough GM, Gualbuerto NC, Pinkner JS, Tamadonfar KO, et al.** (2025) Mechanisms of uropathogenic *E. coli* mucosal association in the gastrointestinal tract. *Sci Adv* **11**(5), eadp7066. doi: 10.1126/sciadv.adp7066 . PMCID: PMC11784811

[3] **Li X, Li Q, He A, Dang M, Zhang Y, et al.** (2025) Disrupting Biofilm Tolerance by Ionic Microbubble-Mediated Copper Ion Surge for Infection Clearance. *ACS nano* **19**(31), 28624–28643. doi: 10.1021/acsnano.5c08035. PMID: 40743484.

[4] **Sroithongkham P, Nittayasut N, Yindee J, Nimsamer P, Payungporn S, et al.** (2024) Multidrug-resistant *Escherichia coli* causing canine pyometra and urinary tract infections are genetically related but distinct from those causing prostatic abscesses. *Sci Rep* **14**(1):11848.doi: doi: 10.1038/s41598-024-62028-9. PMCID: PMC11116460.

[5] **Rodrigues AS, Batista JGS, Rodrigues MÁV, Thipe VC, Minarini LAR, et al.** (2024) Advances in silver nanoparticles: a comprehensive review on their potential as antimicrobial agents and their mechanisms of action elucidated by proteomics. *Front Microbiol* **15**:1440065. doi: 10.3389/fmicb.2024.1440065. PMCID: PMC11325591.

[6] **Ijaz I, Gilani E, Nazir A, Bukhari A.** (2020) Detail review on chemical, physical and green synthesis, classification, characterizations and applications of nanoparticles. *Green Chem Lett Rev* **13**(3), 223-245. doi: 10.1080/17518253.2020.1802517.

[7] **Said A, Abu-Elghait M, Atta HM, Salem SS.** (2024) Antibacterial Activity of Green Synthesized Silver Nanoparticles Using Lawsonia inermis Against Common Pathogens from Urinary Tract Infection. *Appl Biochem Biotechnol* **196**(1): 85–98. doi: 10.1007/s12010-023-04482-1. PMCID: PMC10794286.

[8] **Malaikozhundan B, Mohandoss S, Krishnamoorthi R, Bharathi PV, Palanisamy S, Vinodhini J.** (2024) Enhanced bactericidal, antibiofilm and antioxidative response of *Lawsonia inermis* leaf extract synthesized ZnO NPs loaded with commercial antibiotic. *Bioprocess Biosyst Eng* **47**(8), 1241–1257. doi: 10.1007/s00449-024-03000-9. PMID: 38607416.

[9] **Danaei M, Motaghi MM, Naghmachi M, Amirmahani F, Moravej R.** (2021) Green synthesis of silver nanoparticles (AgNPs) by filamentous algae extract: comprehensive evaluation of antimicrobial and anti-biofilm effects against nosocomial pathogens. *Biologia* **76**, 3057–3069. doi: 10.1007/s11756-021-00808-8 .

[10] **Al-Mutalib LAA, Zgair AK.** (2023) Effect of subinhibitory doses of rifaximin on *in vitro Pseudomonas aeruginosa* adherence and biofilm formation to biotic and abiotic surface models. *Polim Med* **53**(2), 97–103. doi: 10.17219/pim/166584, PMID: 37470308

[11] **Mogessie H, Legesse M, Feleke Haile A, Tesfaye Beyene G, T/Haimanot T, et al.** (2025) Genetic analysis of virulence, extended spectrum beta lactamase, and carbapenem resistance in *Escherichia coli* O157:H7 isolates from drinking water and wastewater in Addis Ababa, Ethiopia. *J Environ Sci Health A Tox Hazard Subst Environ Eng* **60**(7), 342–350. doi: 10.1080/10934529.2025.2596531. PMID: **41352762**

[12] **Shnyoor HA, Zgair AK.** (2025) Effect of combination of sub-inhibitory concentrations of cefepime and Thymus vulgaris essential oil in modulating biofilm formation of *Enterococcus faecalis in vitro*. *Pharm Sci Asia* **52**(3). doi: 10.29090/psa.2025.03.25.3835 .

[13] **Stec J, Kosikowska U, Mendrycka M, Stępień-Pyśniak D, Niedźwiedzka-Rystwej P, et al.** (2022) Opportunistic Pathogens of

Recreational Waters with Emphasis on Antimicrobial Resistance-A Possible Subject of Human Health Concern. *Int J Environ Res Public Health* **19**(12):7308. doi: 10.3390/ijerph19127308. PMCID: PMC9224392.

[14] **Thacharodi A, Ahmed T, Hassan S, Singh PAS, Pugazhendhi A.** (2026) Carbapenem resistance and hypervirulence in *Klebsiella pneumoniae* are raising global public health concerns in the 21st century. *iScience*, **29**(3), 114782. doi: 10.1016/j.isci.2026.114782.

[15] **Mohammed MT, Zgair AK.** (2025) Polymer matrix of biofilm in *Klebsiella pneumoniae* reduced by sub-MIC hydrogen peroxide enhances cefotaxime efficacy. *Polim Med* **55**(2), 113–122. doi: 10.17219/pim/207885. PMID: 41396039.

[16] **Sadiq SI, Ghafil JA.** (2025) Polyhydroxybutyrate nanoparticle improving the sensitivity of Pseudomonas aeruginosa to ceftriaxone and reducing the biofilm formation *in vitro*. *Polim Med* **55**(1): 31–37. doi: 10.17219/pim/203765 , PMID: 40599100.

[17] **Wang H, Shi T, Ma J, Meng S, Wei Z, et al.** (2025) Chitosan-based nanocomposite films incorporated with AgNPs/porphyrinic MOFs for killing pathogenic bacteria. *Int J Biol Macromol* **295**:139584. doi: 10.1016/j.ijbiomac.2025.139584. PMID: 39788251

[18] **Rai M, Ingle AP, Trzcińska-Wencel J, Wypij M, Bonde S, et al.** (2021) Biogenic Silver Nanoparticles: What We Know and What Do We Need to Know?. *Nanomaterials (Basel, Switzerland)* **11**(11), 2901. doi: 10.3390/nano11112901. PMCID: PMC8624974

[19] **Mahale RP, Anuradha K, Princy A, Maheshwarappa YD, Sumana MN.** (2025) Comparative evaluation of biofilm-forming capacity in uropathogenic and commensal *Escherichia coli*. *Front cell Infect Microbiol* **15**:1570422. doi: 10.3389/fcimb.2025.1570422. PMCID: PMC12350247

[20] **Millar BC, Cates MJ, Torrisi MS, Round AJ, Warde A, et al.** (2026) Antimicrobial Resistance: The Answers. *Br J Biomed Sci* **83**:15559. doi: 10.3389/bjbs.2026.15559 . PMCID: PMC12922517.

[21] **Lee SH, Jun BH.** (2019) Silver Nanoparticles: Synthesis and Application for Nanomedicine. *Int J Mol Sci* **20**(4): 865. doi: 10.3390/ijms20040865. PMCID: PMC6412188.

[22] **Rodríguez-Serrano C, Guzmán-Moreno J, Ángeles-Chávez C, Rodríguez-González V, Ortega-Sigala JJ, et al.** (2020) Biosynthesis of silver nanoparticles by *Fusarium scirpi* and its potential as antimicrobial agent against uropathogenic *Escherichia coli* biofilms. *PloS one* **15**(3): e0230275. doi: 10.1371/journal.pone.0230275. PMCID: PMC7067426.

[23] **Sharma D, Misba L, Khan AU.** (2019) Antibiotics versus biofilm: an emerging battleground in microbial communities. *Antimicrob Resist Infect Control* **8**:76. doi: 10.1186/s13756-019-0533-3. PMCID: PMC6524306

[24] **Sahli C, Moya SE, Lomas JS, Gravier-Pelletier C, Briandet R, Hémadi M.** (2022) Recent advances in nanotechnology for eradicating bacterial biofilm. *Theranostics* **12**(5): 2383–2405. doi: 10.7150/thno.67296. PMCID: PMC8899562.

[25] **Kumar L, Bisen M, Harjai K, Chhibber S, Azizov S, et al.** (2023) Advances in Nanotechnology for Biofilm Inhibition. *ACS omega* **8**(24): 21391–21409. doi: 10.1021/acsomega.3c02239. PMCID: PMC10286099

[26] **Dakal TC, Kumar A, Majumdar RS, Yadav V.** (2016) Mechanistic Basis of Antimicrobial Actions of Silver Nanoparticles. *Front Microbiol* **7**: 1831. doi: 10.3389/fmicb.2016.01831. PMCID: PMC5110546.

[27] **Morones JR, Elechiguerra JL, Camacho A, Holt K, Kouri JB, et al.** (2005) The bactericidal effect of silver nanoparticles. *Nanotechnology* **16**(10): 2346–2353. doi: 10.1088/0957-4484/16/10/059.

[28] **Pettersen EF, Goddard TD, Huang CC, Meng EC, Couch GS, et al.** (2021) UCSF ChimeraX: Structure visualization for researchers, educators, and developers. *Protein Sci* **30**(1): 70–82. doi: 10.1002/pro.3943. PMCID: PMC7737788.

[29] **Trott O, Olson AJ.** (2010) AutoDock Vina: improving the speed and accuracy of docking with a new scoring function, efficient optimization, and multithreading. *J Comput Chem* **31**(2): 455–461. doi: 10.1002/jcc.21334. PMCID: PMC3041641.

[30] **Moxon CA, Paulus S.** (2016) Beta-lactamases in Enterobacteriaceae infections in children. *J Infect* **72** *Suppl*: S41–S49. 10.1016/j.jinf.2016.04.021. PMID: 27180312.

[31] **Mohanta YK, Chakrabartty I, Mishra AK, Chopra H, Mahanta S, et al.** (2023) Nanotechnology in combating biofilm: A smart and promising therapeutic strategy. *Front Microbiol* **13**: 1028086. doi: 10.3389/fmicb.2022.1028086. PMCID: PMC10020670.

Author affiliation

1. Department of Biology, College of Science, University of Baghdad, Baghdad, 10071, Iraq
2. Department of Microbiology & Immunology, Georgetown University Medical Center, Washington, D.C.20057, USA.

ORCID IDs:

Ghafil JA: https://orcid.org/0000-0003-1461-302X

Li D: https://orcid.org/0000-0002-3272-2513

Shawi DJ: https://orcid.org/0009-0005-2234-6592

Jaber NA: https://orcid.org/0009-0003-9166-248X